Bioorganic & Medicinal Chemistry 16 (2008) 9511–9518

Contents lists available at ScienceDirect

Bioorganic & Medicinal Chemistry

journal homepage: www.elsevier.com/locate/bmc

Molecular dynamics simulations of the amyloid-beta binding alcohol dehydrogenase (ABAD) enzyme

Alexandra T. Marques, Pedro A. Fernandes, Maria João Ramos *

REQUIMTE, Departamento de Química, Faculdade de Ciências, Universidade do Porto, Rua do Campo Alegre, 687, 4169-007 Porto, Portugal

ARTICLE INFO

Article history:
Received 26 February 2008
Revised 10 September 2008
Accepted 16 September 2008
Available online 19 September 2008

Keywords:
ABAD
AG18051 inhibitor
MM-PBSA
Molecular dynamics

ABSTRACT

In this work, we present 10 ns molecular dynamics simulations of the homotetramer of the ABAD enzyme, as well as of the structural units, dimer and monomer, that assemble to form the tetramer, in the presence and absence of a NAD-inhibitor adduct. The aim was to compare the stability of the different structures and to study the effects of the inhibitor binding on the flexibility of the enzyme structure. The results indicate that the tetramer, dimer and monomer show a comparable stability and that tetramerization stabilizes some regions of the protein that when exposed to the solvent in dimer and monomer become more flexible. Binding of the cofactor and inhibitor stabilizes the protein, the main effect being a stabilization of the substrate binding loop. In the absence of the ligand, this region was found to have a much higher flexibility and to adopt an open conformation. An interesting result emerging from this work is the conformational flexibility exhibited by the azepane and benzene rings of the inhibitor moiety of the adduct, which appears to be influenced by the mobility of the substrate binding loop. This highlights the importance of integrate the flexibility of the substrate binding loop into de novo design of inhibitors of ABAD.

1. Introduction

The enzyme amyloid-beta (Aβ) binding alcohol dehydrogenase (ABAD), also knows as 17β-hydroxysteroid dehydrogenase type 10 (HSD10), is a mitochondrial enzyme which catalyzes the NAD-dependent reversible oxidation and/or reduction of alcohol groups in a wide variety of substrates, comprising linear alcohols, steroids, branched fatty acids, 2-methyl-3-hydroxylbutyryl-coA and β-hydroxybutyrate.[1] This broad substrate specificity of ABAD enables it to participate in several metabolic processes within the mitochondria, namely, the oxidation of fatty acids,[2] degradation of isoleucine,[3] sex steroids metabolism[4,5] and oxidation of steroid modulators of $GABA_A$ receptors.[6]

ABAD is a member of the short-chain dehydrogenase reductase (SDR) family. It forms a homotetramer (Fig. 1a) from two dimers, each assembled by back-to-back association of two subunits.[7,8] Each monomer contains a Rossman fold dinucleotide-binding motif and the Ser/Lys/Tyr catalytic triad characteristic of the SDR enzymes. The most novel aspects of the structure of ABAD arise from the insertion of two loop regions (called insertion-1 and insertion-2) relative to other members of SDR family, which extend from opposite ends of each monomer.

This enzyme has attracted considerable interest because of its ability to interact with the Aβ peptide. Several studies[9–14] suggest this interaction provides a link between A β toxicity and the mitochondrial dysfunction seen in Alzheimer's disease (AD). By interacting with ABAD, Aβ inhibits the normal enzymatic activity of ABAD,[10] promotes oxidative stress[11,12] and induces a signal cascade that lead to apoptosis.[11,12] Structural studies[11,14] about this interaction have demonstrated that Aβ inhibits the ABAD enzymatic activity by inducing a conformational change in ABAD structure which inhibits binding of NAD^+ to the enzyme. The crystal structure of ABAD-Aβ complex[11] reveals the highly distorted ABAD structure, upon Aβ-binding, but provides no molecular details of the interface between ABAD and Aβ due to the lack of electron density of Aβ and of the region of ABAD that binds Aβ. This is perhaps due to the difficulty in obtaining homogeneous, crystalline Aβ protein, even as part of a complex with a better behaved protein. Alternatively, this may simply be due to mobility/disorder in the Aβ-binding region of ABAD, for example. The disordering of the insertion-1 loop, also know as loop L_D, raised the possibility that this region could be the binding site for Aβ. Subsequent site directed mutagenesis studies[11] confirmed that L_D loop plays a critical role in Aβ-binding. A synthesized peptide encompassing the residues from this loop inhibited ABAD-Aβ interaction and when added to cultured neurons of transgenic mice overexpressing ABAD and Aβ, oxidative stress and apoptosis were inhibited.[11] Overall, this data indicates that the ABAD-Aβ interaction is a

* Corresponding author. Tel.: +351 226082806; fax: +351 226082959.
E-mail address: mjramos@fc.up.pt (M.J. Ramos).

0968-0896/$ - see front matter © 2008 Elsevier Ltd. All rights reserved.
doi:10.1016/j.bmc.2008.09.043

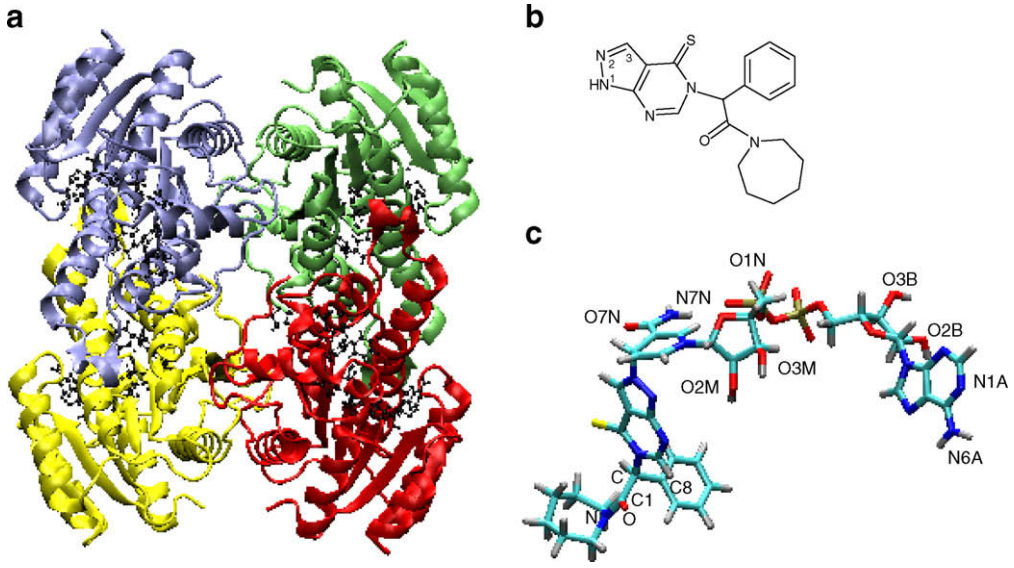

Figure 1. (a) Tetrameric structure of ABAD in complex with the NAD-inhibitor adduct (pdb: 1U7T). The ligand is represented in ball-and-stick. (b) Structure of the AG18051 (1-azepan-1-yl-2-phenyl-2-(4-thioxo-1,4-dihydro-pyrazolo[3,4-d]pyrimidin-5-yl)-ethanone) inhibitor. (c) Structure of the adduct formed between the inhibitor AG18051 and the cofactor NAD^+. The N2 atom of the inhibitor is covalently linked to the C4N atom of the nicotinamide ring of NAD^+.

potential target for drug development for treatment of AD. In this way, the search for inhibitors of the ABAD-Aβ interaction has already started and a class of benzothiazole ureas have been recently identified.[15]

An inhibitor against human ABAD was also developed.[8] This pyrazolo-thionopyrimidine-based inhibitor (Fig. 1b) is the only known inhibitor of the enzyme and was developed as part of a structure-based drug design project, with the aim to be used in the research of ABADs roles both in normal cellular conditions and in AD pathogenesis. The crystal structure of the ABAD in complex with the cofactor and the inhibitor revealed that the N2 atom of the inhibitor reacts with the C4N atom of NAD^+, leading to formation of a tightly bound NAD-inhibitor adduct (Fig. 1a and c). In this work, we have performed molecular dynamics simulations of the tetramer, dimer and monomer of the ABAD, in the presence and absence of this ligand. The aim was to compare the stability of the different structures and to study the effects of the inhibitor binding on the flexibility of the enzyme structure. The information gleaned from these studies might be useful for the rational design of novel inhibitors of ABAD.

2. Results

2.1. Protein structural features

To assess the stability of the ABAD structures during the MD simulations, the backbone RMSD values with respect to the initial structures were calculated along the 10 ns trajectories and are shown in Figure 2. From this figure, we can be seen that the RMSDs of the complexed structures are low and remain stable after an initial period of equilibration. The RMSD of the complexed tetramer remains around 1.2 Å after the first 2.5 ns while the RMSD of the complexed dimer remains around 1.4 Å after the first 1 ns. In both cases, the individual monomers exhibit similar stabilities. The RMSD of the complexed monomer was also very stable, oscillating around 1.4 Å during the simulation time. These results indicate that the complexed structures show a comparable stability during the explored timescale of 10 ns. In comparison with the complexed structures, the uncomplexed structures display higher deviations during the simulation time. Visual inspection of the simulations revealed that this is mainly due to an increase in the flexibility of the substrate binding loop in the absence of the ligand. After the 6 ns, the flexibility of this region began to increase more pronouncedly in three monomers of the uncomplexed tetramer, leading their RMSDs to increase up to 2.5 Å in the last 2 ns of the simulation time. At about 2 ns, the RMSDs of the dimer and individual monomers jump ~1 Å, also due to a large increase in the mobility of their substrate binding loops. The increase in the RMSD of uncomplexed monomer between 5 and 7 ns is also derived from an increase in the flexibility of the substrate binding loop.

In Figure 3 is shown the superposition of one monomer of the ABAD crystal structure with the average structures, over the last 2 ns, of one monomer of the tetrameric and dimeric structures and of the isolated monomeric structures. From this figure it is possible to see that in the absence of the ligand, the substrate binding loop moves away, opening up the substrate binding cavity. This outward movement of the substrate binding loop lead to an expansion of the protein and hence, to changes in the gyration radius. As can be seen in Figure 4, the gyration radius is very stable for the complexed structures. However, in case of the uncomplexed structures, the radius of gyration increases when the RMSD increases due to motion of the substrate binding loop.

The secondary structure was also monitored along the MD trajectories. In all the structures the secondary structure elements were well maintained (data not shown). The short αEF helix (residues 157–160) and two 3–10 right-handed helices (residues 187–189, 204–208), one of them located in the substrate binding loop, were an exception, demonstrating a lower stability.

In order to obtain a more detailed description of the flexibility of the different structures, the RMS fluctuations of the backbone atoms were calculated over the last 2 ns and are shown in Figure 5. In this figure, the experimental values (average of the monomers of the crystal structure) derived from the crystallographic B-factors are also shown and the positions of important regions of ABAD are indicated. Although the magnitude of the experimental values is generally higher than the magnitude of values calculated from the MD simulations, there is a relatively good agreement in the fluctuation pattern, especially with the complexed structures. Comparison of RMS fluctuations between complexed and uncomplexed structures, shows that there is an overall increase in protein

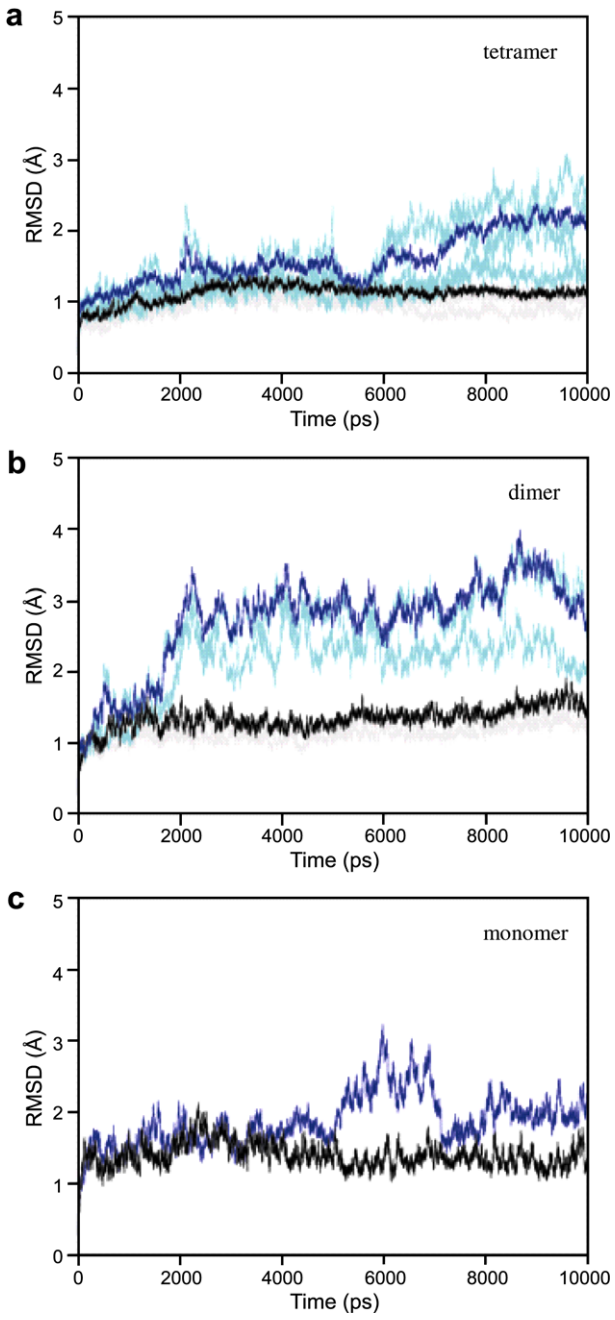

Figure 2. Backbone RMSD as a function of time (with respect to the initial structure) for the MD simulations of tetrameric (a), dimeric (b) and monomeric (c) structures. In dark blue is the RMSD for the uncomplexed structures and in black is the RMSD for the complexed ones. In light blue is the RMSD for the individual monomers of the uncomplexed tetrameric and dimeric structures. In grey is the RMSD for the individual monomers of the complexed tetrameric and dimeric structures.

flexibility in the absence of the ligand and confirms that the largest change in flexibility occurs in the substrate binding loop. In case of the tetramer, the other regions showing a clear increase in flexibility in the absence of the ligand are mainly located in the N-terminal part of the enzyme and make part of the cofactor binding cavity. In comparison with the tetrameric structures, the monomeric and dimeric structures display an increase in the flexibility of the C-terminal residues immediately after the substrate binding loop region in protein sequence. In the tetramer most of these residues are buried in the interface between the two dimers and hence, are quite rigid. The monomeric structures also exhibit an increase in the flexibility of residues 156–166 from the substrate binding cavity and this is because these residues, which normally lie in the dimer interface, became solvent exposed in monomer. Another region that has a higher flexibility in monomeric structures is the insertion-1 loop and the motion of this loop is shown in Figure 3. Again, this is related with the fact of many residues of the insertion-1, which normally lie at the dimer interface, become completely exposed to the solvent in the monomer and hence see their mobility increased.

2.2. Conformational changes in the inhibitor

Figure 6 shows the RMSD of the NAD-inhibitor adduct along the 10 ns trajectories. From this figure it is possible to see that the ligands bound to tetramer and dimer exhibit jumps of ~1 Å or higher in their RMSDs at different simulation times, suggesting the existence of conformational changes. In case of the tetramer these conformational changes start to occur only after the first 1 ns while for one of the ligands bound to the dimer they start at the very beginning of the simulation. In contrast, the RMSD of the ligand bound to the monomer is more stable, fluctuating around 1 Å during the entire simulation time.

Visual inspection of the trajectories revealed that the jumps in the RMSDs of the ligands are associated with changes in the conformation of the inhibitor part of the adduct, namely, at level of the azepane and benzene rings. This is illustrated in Figure 7 which shows the crystal structure of one monomer with the bound adduct superposed with average structures, calculated for each 1 ns of the trajectory, of one monomer of the complexed tetramer. Interestingly, the conformational flexibility of the azepane and benzene rings appears to be related with the flexibility of the substrate binding loop. From Figure 7 it is possible to see that, excepting the average structure over the first 1 ns, the other structures show a small movement of the substrate binding loop away the binding cavity, creating space around the benzene ring. This space is then used by this ring to rotate around the C–C8 single bond (Fig. 1c) in order to achieve a conformation that keeps the hydrophobic interactions with the substrate binding loop, namely, with Leu209. The azepane ring is very flexible, easily changing its conformation through a bending motion and/or rotation around the N–C1 single bond (Fig. 1c). When it completely changes its orientation toward the part of the active site, that is, more accessible to the solvent, the hydrophobic contacts with Leu217, Leu209 and Val213 from the substrate binding loop are lost.

It is also interesting to note that, in case of the isolated monomer, this conformational flexibility of the benzene and azepane rings is not observed during the explored timescale, as shown in Figure 7c. This may be explained by the smaller outward movement of the substrate binding loop in this structure relatively to those observed in the other structures (see Fig. 3). However, it is possible that these conformational changes could be observed for the monomer by extending the simulation time, as in case of the tetramer, they started to occur later for one of the bound ligands (ligand showed in green in Fig. 6).

2.3. Hydrogen bonds protein–ligand

The hydrogen bonds between the protein and the ligand were monitored during the MD simulations and Table 1 summarizes those with occupancies above 50%. From this table it is possible to see that the dimer and monomer show similar occupancies for the hydrogen bonds with the adduct to those found for the tetramer (Table 1), indicating that, despite some differences in the stability of these structures, the conformations of residues from the binding cavity are similar. Of the hydrogen bonds listed in

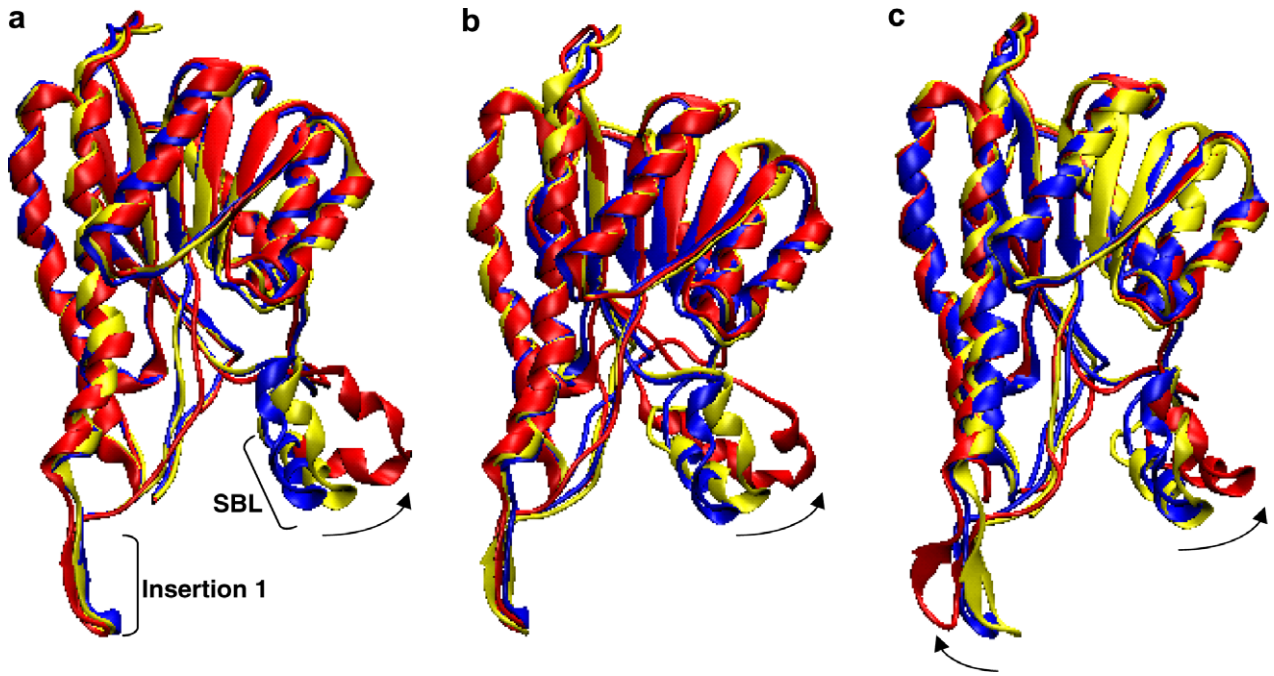

Figure 3. Superposition of one monomer of the ABAD crystal structure 1U7T (blue) with the average structures over the last 2 ns of one monomer of the complexed (yellow) and uncomplexed (red) tetramer (a) and dimer (b) and of the complexed (yellow) and uncomplexed (red) isolated monomer (c). SBL, substrate binding loop.

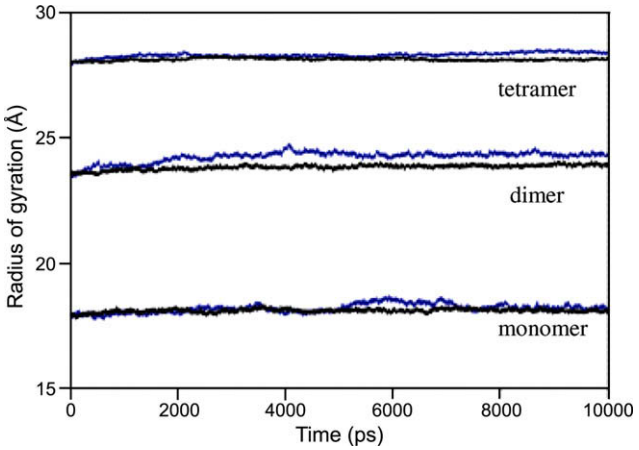

Figure 4. Radius of gyration as a function of simulation time for the complexed (black) and uncomplexed (blue) tetramer, dimer and monomer.

Table 1, one is mediated by the inhibitor moiety of the adduct (between carbonyl oxygen atom and Gln165) and the others are mediated by the cofactor moiety. The conformation of NAD^+ is not altered with adduct formation beyond movement of the C4 N atom out of the plane of the nicotinamide ring,[8] and hence, many of the hydrogen bonds with NAD^+, characteristic of the SDR family, are observed with a high occupancy. The Asp41, whose positioning in the cofactor binding pocket is responsible for the discrimination for NADH over NADPH, makes hydrogen bonds with both hydroxyl groups of the adenine ribose. Residues Val65 and Asp64 interact with the adenine moiety while Phe201 stabilizes the nicotinamide ring by making hydrogen bonds with the carboxamide group. Residue Thr203 makes a strong hydrogen bond with one phosphoryl oxygen. Residues Cys91, Ala92, Lys172 and Tyr168 interact with the nicotinamide ribose. The interaction between the Lys172 and the 3′-OH group of the nicotinamide ribose has an important role in orientating the coenzyme to allow only pro-(S)-hydride transfer, a feature common to SDR enzymes. The hydrogen bond between the hydroxyl group of Tyr168, the proton donor in catalysis, and the 2′-OH group of the nicotinamide ribose, brings the tyrosine in close proximity to this ring, which is the site of hydride transfer. In the crystal structure, the inhibitor forms a second hydrogen bond, through its N1 atom, with the hydroxyl group of Tyr168. Based on this interaction, Tyr168 was proposed to mediate the adduct formation, by extracting a proton from the N1 atom of the inhibitor in a similar way when it extracts a proton from the hydroxyl group of a bound substrate. The N2 atom of the AG18051 may acquire a negative charge through charge delocalization and then nucleophilically attack the C4N position of the NAD^+ nicotinamide ring to form a covalent bond. The hydrogen bond between the hydroxyl group of Tyr168 and the N1 atom of the inhibitor showed however a very small occupancy (less than 30%). This suggests that in the mechanistic context the hydrogen bond between Tyr168 and the N1 atom is important only in the pre-catalytic complex, where the pyrazole ring may have another orientation because it is not yet bound to the nicotinamide ring of NAD.

2.4. Binding energy protein–ligand

To compare the affinities of the ligand to the tetramer, dimer and monomer, relative binding energy difference between the ligand bound to the monomer and the ligands bound to the tetramer and dimer were calculated with the MM-PBSA method. The last 2 ns of the trajectories were used in the calculations and the results are summarized in Table 2. Analysis to this table reveals that there is an asymmetry in the binding energies obtained for the ligands bound to the tetramer and to the dimer. In both structures, one of the ligands has a higher (i.e., more negative) binding affinity, similar to that obtained for the ligand bound to the monomer. In case of the tetramer, the binding energies differ in a maximal value of 5.30 kcal/mol and in case of the dimer they differ in 6.44 kcal/mol. Given the larger size of the adduct, this asymmetry may be considered relatively small. It appears to be not directly related with the different conformations assumed by the inhibitor part

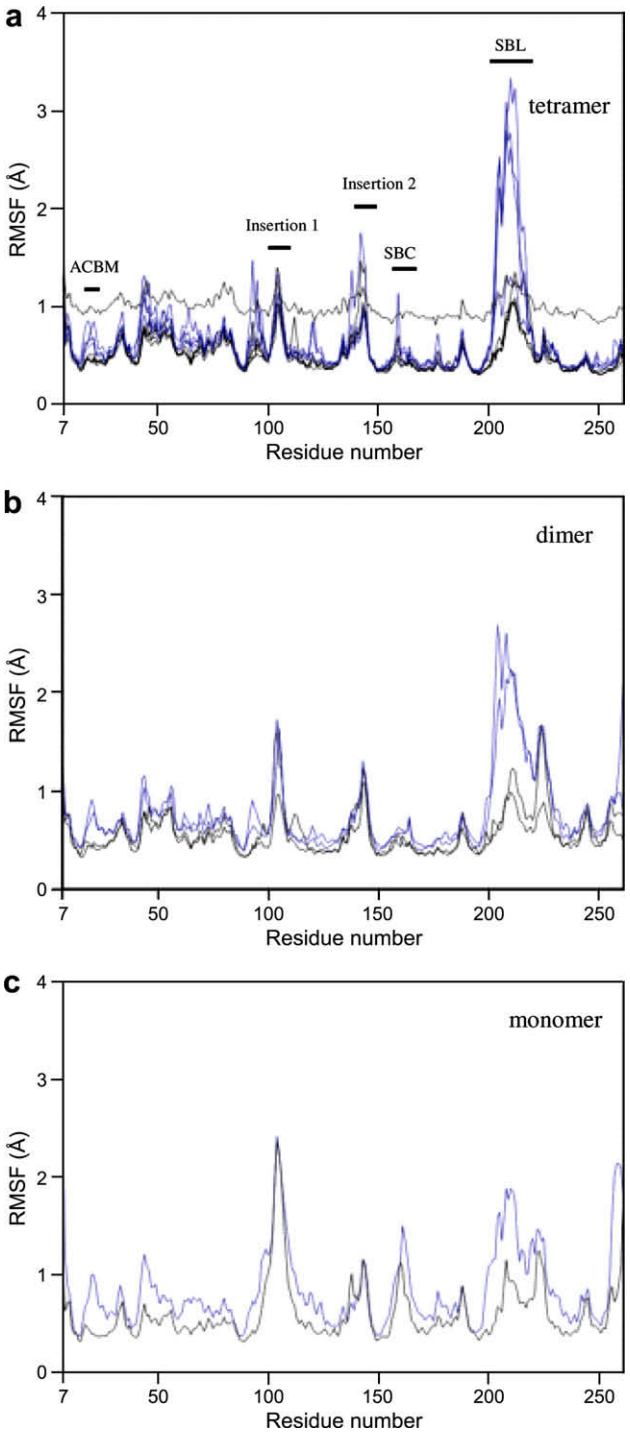

Figure 5. RMS fluctuations of backbone (evaluated for the last 2 ns) for the tetramer (a), dimer (b) and monomer (c). The RMS fluctuations for complexed monomers are in black and for the uncomplexed monomers are in blue. The experimental RMS fluctuations, derived from the crystallographic B-factors are shown in dashed line. ACBM, adenine cofactor binding motif; SBC, substrate binding cavity; SBL, substrate binding loop.

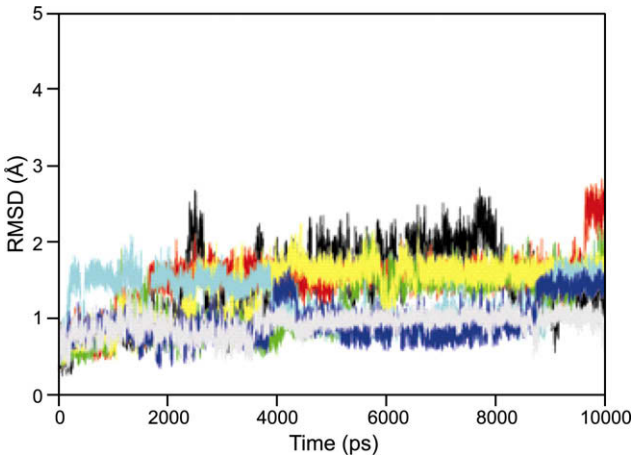

Figure 6. (a) RMSD as a function of time for the ligand bound to the monomer (grey) and for the ligands bound to the tetramer (black, red, yellow and green) and dimer (dark and light blue).

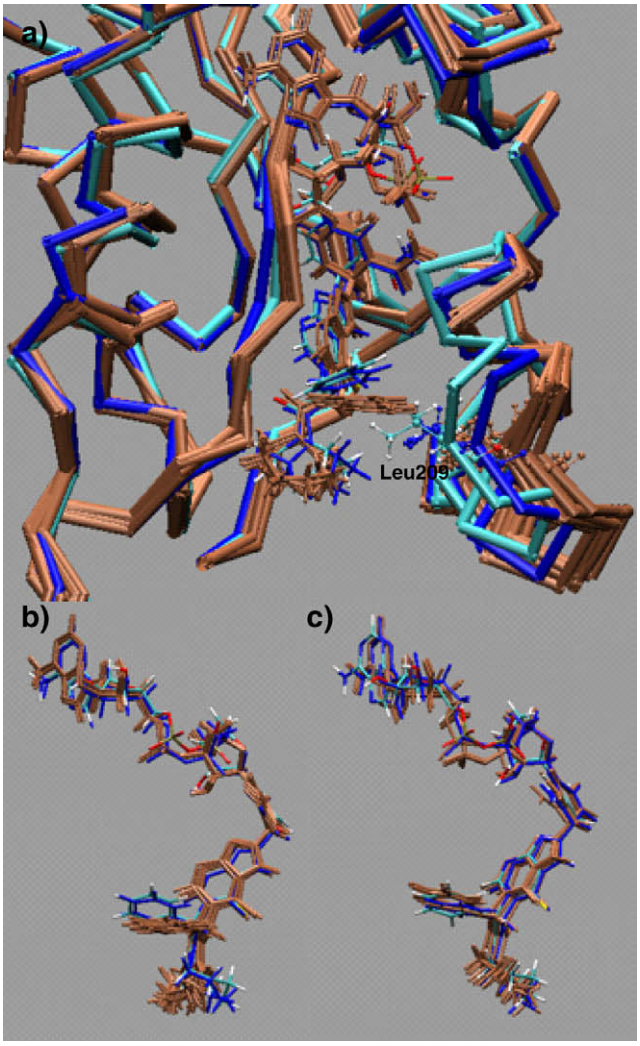

Figure 7. (a) Superposition of one monomer with bound adduct of the crystal structure of ABAD 1U7T with the average structures over each 1 ns of one of the monomers of the complexed tetramer. The crystal structure is colored by atom, the average structure over the first 1 ns is in dark blue and the other average structures are in brown. (b) Another view of the ligand shown in (a). (c) Average structures over each 1 ns of the ligand bound to the isolated monomer.

of the ligand as in the last 2 ns the ligands bound to the dimer exhibit a similar trend in their RMSDs. Also, the calculation of the relative binding energies considering the first 1 ns of the simulation, a period where the conformations of the ligands bound to the tetramer and monomer are very similar and similar to that of the crystal structure, also reveal an asymmetry in the binding energies of the ligands bound to the tetramer (values of relative binding energy

Table 1
Hydrogen bonds between the NAD-inhibitor adduct and ABAD structures with >50% occupancies during the simulation time

Protein	Adduct[a]	Occupancy (%)						
		Tetramer				Dimer		Monomer
		1	2	3	4	1	2	
Acceptor	*Donor*							
Asp41-OD2	O3B	99.98	99.42	99.94	67.98	99.81	99.62	99.87
Asp41-OD1	O2B	99.99	99.97	99.96	99.92	99.99	99.93	100.00
Asp41-OD1	O3B	65.84	60.44	66.08	87.63	69.95	57.19	<50
Asp64-OD2	N6A	68.67	58.8	59.68	66.54	63.53	50.06	50.40
Cys91-O	O3M	73.13	<50	80.53	54.63	57.43	<50	61.71
Ala92-O	O3M	62.40	82.68	53.66	65.05	82.86	87.91	72.22
Donor	*Acceptor*							
Val65-N	N1A	99.90	99.98	99.90	99.94	99.95	99.97	99.89
Gln165-NE2	O	85.09	91.37	89.29	96.34	93.69	99.68	98.09
Tyr168-OH	O2M	82.06	86.60	80.94	65.13	86.52	<50	99.59
Lys172-NZ	O3M	97.64	94.76	90.80	81.87	99.14	92.68	98.92
Lys172-NZ	O2M	86.92	92.54	84.95	95.16	82.72	91.21	75.61
Phe201-NH	O7N	99.78	99.82	99.48	99.78	98.83	98.34	90.05
Thr203-OG1	O1N	99.85	98.62	99.59	97.99	98.55	75.30	73.27

[a] The localization of these atoms in the adduct structure is shown in Figure 1c.

Table 2
Relative binding free energy components of the ligands bound to the tetramer and dimer relative to the ligand bound to the isolated monomer (kcal/mol)

Structure	$\Delta\Delta E_{ele}$	$\Delta\Delta E_{vdw}$	$\Delta\Delta G_{SA}$	$\Delta\Delta G_{PB}$	$\Delta\Delta G_{binding}$
Tetramer					
Monomer1	1.36 ± 0.49	5.73 ± 0.71	0.52 ± 0.02	0.21 ± 0.49	7.40 ± 0.60
Monomer2	−2.12 ± 0.46	9.74 ± 0.71	0.48 ± 0.02	−2.74 ± 0.44	5.36 ± 0.60
Monomer3	−5.46 ± 0.48	1.10 ± 0.65	0.19 ± 0.02	7.52 ± 0.46	3.34 ± 0.57
Monomer4	−9.92 ± 0.52	6.45 ± 0.69	0.38 ± 0.02	5.18 ± 0.50	2.10 ± 0.59
Dimer					
Monomer1	−4.18 ± 0.53	5.55 ± 0.68	0.30 ± 0.02	4.76 ± 0.46	6.44 ± 0.94
Monomer2	5.74 ± 0.50	2.50 ± 0.71	0.14 ± 0.02	−8.06 ± 0.49	0.33 ± 0.94

vary between 0.77 and −2.95 kcal/mol). This could result from the existence of cooperativity between the binding sites in tetramer. However, at least in case of the substrates allopregnanolone and allotetrahydrodeoxycorticosterone no cooperativity was observed.[6]

3. Discussion

In this work, we report 10 ns MD simulations of the ABAD tetramer as well as of the structural units (monomer and dimer) that assemble to form the tetramer. The crystal structure of ABAD in complex with a NAD-inhibitor adduct was used to obtain the starting structures and the simulations were performed both in the presence and absence of the ligand. The aim was to compare the stability of dimer and monomer with that of tetramer and to study the effects of the inhibitor binding on the flexibility of the enzyme structure. Overall, the results indicate that the dimer and monomer show a comparable stability with that of tetramer. Some regions of the protein are however more stabilized upon tetramerization given that when exposed to the solvent in dimer and monomer they become more flexible. These regions include the insertion-1 loop, the C-terminal residues located in the interface between the two dimers in the tetramer, and some residues of the binding cavity normally located in the dimer interface. Binding of the cofactor and inhibitor stabilizes the structures, namely the substrate binding loop. In the absence of the ligand, this region showed a much higher flexibility and a movement away from the binding cavity. A mobile substrate binding loop is present in other members of the SDR family and is reported to undergo conformational changes upon substrate binding. This region has been shown to adopt different conformations in SDR enzymes, depending on the presence/absence of the cofactor or substrate.[16–18] In case of ABAD, insights into conformational changes in the substrate binding loop upon substrate binding were obtained from the comparison of the crystal structures of the rat ABAD[7] as a binary complex with NADH, as a ternary complex with NAD^+ and acetoacetate, and as a ternary complex with NAD^+ and 17β-estradiol. The substrate binding loop is disordered in the first crystal structure, keeps disordering in the presence of 17β-estradiol but becomes ordered in the presence of acetoacetate. A structure of the ABAD apoenzyme is not yet available and hence, the mechanism of loop closure in this enzyme cannot be completely delineated. Our MD simulation of the uncomplexed tetramer (i.e., apoenzyme) shows a conformational transition of the substrate binding loop from a closed to an open conformation. Despite the disordering of the substrate binding loop in all subunits of the binary complex with NAD^+, one of the subunits with bound NAD^+ of the ternary complex with 17β-estradiol and NAD^+ displayed the substrate binding loop in a ordered and closed conformation. Taken together, this data seems to suggest that the substrate binding loop may be in the open conformation in the ABAD apoenzyme and that loop closure may be induced by NAD^+ binding alone.

An interesting result emerging from this work is the conformational flexibility exhibited by the azepane and benzene rings of the inhibitor moiety of the adduct, which appears to be related with the mobility of the substrate binding loop. During the simulation of the complexed structures, the substrate binding loop moves to a more open conformation, leading to the weakening or loss of the hydrophobic interactions with the azepane and benzene rings of the inhibitor. The azepane ring sample many conformations, while the benzene ring reorientates inside the more spacious binding cavity in order to keep the hydrophobic interactions with the

loop. These results highlight the importance of integrate the flexibility of the substrate binding loop into de novo design of inhibitors of ABAD.

In structure-based drug design studies, where generally many ligands are tested and ranked according to their binding energies, the use of a small part of a large protein system may allow to save considerable computational time. In this sense, the used of a monomer of ABAD in this type of studies is tempting. Our MD simulations revealed that the tetramer and monomer exhibit similar stability, similar protein-adduct hydrogen bonding pattern and relatively similar protein–ligand binding energies. However, the substrate binding loop is not so flexible in the monomer and because of this the conformational changes in the inhibitor were not observed during the explored timescale. Taken together, these results suggest that the isolated monomer may be used as a simplified model of ABAD but with some limitations.

4. Materials and methods

4.1. Model setup

The X-ray crystallographic structure of ABAD complexed with the NAD-AG18051 adduct (Protein Data Bank entry 1U7T)[11] was used to obtain the starting structures for the MD simulations. In this structure the inhibitor is bound only in three of the four monomers, as the fourth monomer is involved in a crystal packing interaction which leads to a narrowing of the binding cleft, precluding inhibitor binding. Thus, the fourth monomer was replaced by one of the others in order to obtain the complete tetramer. The first six amino acids of each monomer were not resolved in the crystal due to the absence of electron density. The incomplete side-chains of twelve amino acids were reconstructed with the Biopolymer module of InsightII software.[19] Standard physiological protonation states were attributed to all amino acids (deprotonated Glu and Asp, protonated Lys and Arg, remaining amino acids neutral).

The structure of the complexed dimer and monomer were obtained through deletion of one of the dimers and of three monomers in the tetramer structure, respectively. The structures of the uncomplexed tetramer, dimer and monomer were obtained through deletion of the ligand(s). All the six structures of ABAD were subjected to molecular dynamics.

4.2. Molecular dynamics

All simulations were done with the AMBER 8.0[20] software and the *Cornell* force field[21] was used for the protein. The antechamber program, in combination with the general amber force field,[22] was used to generate parameters for the ligand. The atomic point charges of the ligand were determined using the restrained electrostatic potential (RESP) procedure,[23] based on HF/6-31* calculations conducted with Gaussian03 program.[24] After addition of hydrogen atoms with the program Xleap, the structures were charge neutralized and then solvated by a truncated octahedron of TIP3P waters with a minimum of 16 Å (monomeric structures) or 20 Å (dimeric and tetrameric structures) water layer between the octahedron edges and the nearest solute atoms. The structures were energy minimized in three consecutive rounds, each of which consisting in 5000 steps (2000 of steepest-descent and 3000 of conjugate gradient). Positional restraints on the heavy atoms and protein main-chain atoms (C_α, C, N) were applied in the first and second rounds, respectively. In the third round the whole system was minimized. After full relaxation, the structures were heated up from 0 K to 300 K in 50 ps. Finally, 10 ns of MD simulations at 300 K and 1 atm were carried out. Bond lengths involving hydrogens were constrained using the SHAKE algorithm,[25] and the equations of motion were integrated with a 2-fs time step. The nonbonded cutoff distance was 10 Å and the Particle Mesh Ewald (PME) method[26] was used to calculate the full electrostatic energy of the periodic simulation cell in an infinite lattice of repeating images. The temperature of the system was regulated using the Langevin thermostat.[27]

4.3. Analysis

The Ptraj module of Amber 8.0[20] and the VMD[28] program were used for all the analyses. The gyration radius and the root mean-square deviation (RMSD) of the backbone atoms from the initial structure were calculated for the different trajectories. For each trajectory, the average structure was calculated after mass weighted backbone RMS fit of every frame to the first frame in the trajectory to remove translational and rotational motion. Root mean-square (RMS) fluctuations of the C_α atoms were calculated for the last 2 ns of the MD trajectories after removal of translational and rotational motion of the ABAD structures. The hydrogen bonds were computed according to the following criteria: (1) the distance between proton donor (*X*) and acceptor (*Y*) atoms was less than or equal to 3.5 Å, (2) the angle *X*–H...*Y* was greater than or equal to 120°.

The relative binding energy difference between the ligand bound to the monomer and the ligands bound to the tetramer and dimer was calculated as:

$$\Delta\Delta G_{\text{binding}} = \Delta G_{\text{isolated monomer}} - \Delta G_{\text{monomer in tetramer/dimer}} \quad (1)$$

The MM-PBSA method,[29] implemented in AMBER8, was used to estimate the binding free energies of the ligand to the different ABAD structures. In the MM-PBSA approach, the binding free energy of a ligand is calculated as the difference between the free energies of the complex and the separate monomers (protein and free ligand):

$$\Delta G_{\text{binding}} = G_{\text{complex}} - (G_{\text{protein}} + G_{\text{ligand}}) \quad (2)$$

The free energy of each species (complex, protein and ligand) is calculated by summing the internal energy (bond, angle and dihedral), the electrostatic and the van der Waals interactions, the free energy of polar solvation, the free energy of nonpolar solvation, and the entropic contribution for the molecule free energy:

$$G_{\text{molecule}} = E_{\text{int}} + E_{\text{ele}} + E_{\text{vdw}} + G_{\text{PB}} + G_{\text{SA}} - \text{TS} \quad (3)$$

The last 2 ns were used to calculate these energy terms. The Sander program was used to calculate the first three terms in Eq. (3), which represent the molecular mechanics energy. The nonpolar contribution to the solvation free energy was estimated from the equation: $G_{SA} = \gamma\text{SASA} + b$, where SA is the solvent-accessible surface area calculated with the Molsurf program. The empirically determined parameters γ and b are 0.00542 kcal mol^{-1} Å^{-2} and 0.92 kcal mol^{-1}, respectively.[30] The polar contribution to the solvation free energy was calculated by solving the Poisson–Boltzmann equation with the program Delphi.[31] The interior dielectric constant was set to 4 as the experimental value of dielectric constant for proteins is ~4. The exterior dielectric constant was set to 80.0. The entropy contribution for the binding energy is expected to be very similar for the ligand in complex with the monomer, dimer and tetramer and hence, to cancel out when computing the $\Delta\Delta G_{\text{binding}}$.

Acknowledgments

A.T. Marques was supported by a Ph.D. grant (SFRH/BD/19228/2004) from Fundação para a Ciência e a Tecnologia.

References and notes

1. Yang, S. Y.; He, X. Y.; Schulz, H. *Trends Endocrinol. Metab.* **2005**, *16*, 167.
2. He, X. Y.; Schulz, H.; Yang, S. Y. *J. Biol. Chem.* **1998**, *273*, 10741.
3. Ofman, R.; Ruiter, J.; Feenstra, M.; Duran, M.; Toll-The, B.; Zschocke, J.; Ensenauer, R.; Lehnart, W.; Sass, J.; Sperl, W.; Wanders, R. *Hum. Genet.* **2003**, *72*, 1300.
4. He, X. Y.; Yang, Y. Z.; Peehl, D. M.; Lauderdale, A.; Schulz, H.; Yang, S. Y. *J. Steroid Biochem. Mol. Biol.* **2003**, *87*, 191.
5. Ivell, R.; Balvers, M.; Anand, R. J.; Paust, H. J.; Mckinnell, C.; Sharpe, R. *Endocrinology* **2003**, *144*, 3130.
6. He, X. Y.; Wegiel, J.; Yang, S. Y.; Pullarkat, R.; Schulz, H.; Yang, S. Y. *Mol. Cell. Endocrinol.* **2005**, *229*(1–2), 111.
7. Powell, A. J.; Read, J. A.; Banfield, M. J.; Gunn-Moore, F.; Yan, S. D.; Lustbader, J.; Stern, A. R.; Stern, D. M.; Brady, R. L. *J. Mol. Biol.* **2000**, *303*, 327.
8. Kissinger, C. R.; Rejto, P. A.; Pelletier, L. A.; Thomson, J. A.; Showalter, R. E.; Abreo, M. A.; Agree, C. S.; Margosiak, S.; Meng, J. J.; Aust, R. M.; Vanderpool, D.; Li, B.; Tempczyk-Russell, A.; Villafranca, J. E. *J. Mol. Biol.* **2004**, *342*, 943.
9. Yan, S. D.; Fu, J.; Soto, C.; Chen, X.; Zhu, H.; Al-Mohanna, F.; Collison, K.; Zhu, A.; Stern, E.; Saido, T.; Tohyama, M.; Ogawa, S.; Roher, A.; Stern, D. *Nature* **1997**, *389*, 689.
10. Yan, S. D.; Shi, Y.; Zhu, A.; Fu, J.; Zhu, H.; Zhu, Y.; Gibson, L.; Stern, E.; Collison, K.; Al-Mohanna, F.; Ogawa, S.; Roher, A.; Clarke, S. G.; Stern, D. M. *J. Biol. Chem.* **1999**, *274*, 2145.
11. Lustbader, J. W.; Cirilli, M.; Lin, C.; Xu, H. W.; Takuma, K.; Wang, N.; Caspersen, C.; Chen, X.; Pollak, S.; Chaney, M.; Trinchese, F.; Liu, S.; Gunn-Moore, F.; Lue, L. F.; Walker, D. G.; Kuppusamy, P.; Zewier, Z. L.; Arancio, O.; Stern, D.; Yan, S. S.; Wu, H. *Science* **2004**, *304*, 448.
12. Takuma, K.; Yao, J.; Xu, H.; Chen, X.; Luddy, J.; Trillat, A. C.; Stern, D. M.; Arancio, O.; Yan, S. S. *FASEB J.* **2005**, *19*, 597.
13. Yan, S. D.; Stern, D. M. *Int. J. Exp. Pathol.* **2005**, *86*, 161.
14. Yan, Y.; Liu, Y.; Sorci, M.; Belfort, G.; Lustbader, J. W.; Yan, S. S.; Wang, C. *Biochemistry* **2007**, *46*, 1724.
15. Xie, Y.; Deng, S.; Chen, Z.; Yan, S.; Landry, D. W. *Bioorg. Med. Chem. Lett.* **2006**, *16*, 4657.
16. Grimm, C.; Maser, E.; Mobus, E.; Klebe, G.; Reuter, K.; Ficner, R. *J. Biol. Chem.* **2000**, *275*, 41333.
17. Youn, B.; Moinuddin, S. G.; Davin, L. B.; Lewis, N. G.; Kang, C. *J. Biol. Chem.* **2005**, *280*(13), 12917.
18. Paithankar, K. S.; Feller, C.; Kuettner, E. B.; Keim, A.; Grunow, M.; Sträter, N. *FEBS J.* **2007**, *274*(21), 5767.
19. InsightII, Accelrys Inc.: San Diego, CA, U.S.A., 2005.
20. Case, D. A.; Darden, T. A.; Cheatham, T. E., III; Simmerling, C. L.; Wang, J.; Duke, R. E.; Luo, R.; Merz, K. M.; Wang, B.; Pearlman, D. A.; Crowley, M.; Brozell, S.; Tsui, V.; Gohlke, H.; Mongan, J.; Hornak, V.; Cui, G.; Beroza, P.; Schafmeister, C.; Caldwell, J. W.; Ross, W. S.; Kollman, P. A. Amber 8, University of California: San Francisco, 2004.
21. Cornell, W. D.; Cieplak, P.; Bayly, C. I.; Gould, I. R.; Merz, K. M.; Ferguson, D. M.; Spellmeyer, D. C.; Fox, T.; Caldwell, J. W.; Kollman, P. A. *J. Am. Chem. Soc.* **1995**, *117*, 5179.
22. Wang, J.; Wolf, R. M.; Caldwell, J. W.; Kollman, P. A.; Case, D. A. *J. Comput. Chem.* **2004**, *25*, 1157.
23. Cieplak, P.; Cornell, W. D.; Bayly, C.; Kollman, P. A. *J. Comput. Chem.* **1995**, *16*, 1357.
24. Frisch, M. J.; Trucks, G. W.; Schlegel, H. B.; Scuseria, G. E.; Robb, M. A.; Cheeseman, J. R.; Montgomery, J. A., Jr.; Vreven, T.; Kudin, K. N.; Burant, J. C.; Millam, J. M.; Iyengar, S. S.; Tomasi, J.; Barone, V.; Mennucci, B.; Cossi, M.; Scalmani, G.; Rega, N.; Petersson, G. A.; Nakatsuji, H.; Hada, M.; Ehara, M.; Toyota, K.; Fukuda, R.; Hasegawa, J.; Ishida, M.; Nakajima, T.; Honda, Y.; Kitao, O.; Nakai, H.; Klene, M.; Li, X.; Knox, J. E.; Hratchian, H. P.; Cross, J. B.; Bakken, V.; Adamo, C.; Jaramillo, J.; Gomperts, R.; Stratmann, R. E.; Yazyev, O.; Austin, A. J.; Cammi, R.; Pomelli, C.; Ochterski, J. W.; Ayala, P. Y.; Morokuma, K.; Voth, G. A.; Salvador, P.; Dannenberg, J. J.; Zakrzewski, V. G.; Dapprich, S.; Daniels, A. D.; Strain, M. C.; Farkas, O.; Malick, D. K.; Rabuck, A. D.; Raghavachari, K.; Foresman, J. B.; Ortiz, J. V.; Cui, Q.; Baboul, A. G.; Clifford, S.; Cioslowski, J.; Stefanov, B. B.; Liu, G.; Liashenko, A.; Piskorz, P.; Komaromi, I; Martin, R. L.; Fox, D. J.;. Keith, T.; Al-Laham, M. A.; Peng, C. Y.; Nanayakkara, A.; Challacombe, M.; Gill, P. M. W.; Johnson, B.; Chen, W.; Wong, M. W.; Gonzalez, C.; Pople, J. A.; Gaussian 03, Inc., Wallingford, CT, 2004.
25. Ryckaert, J. P.; Ciccotti, G.; Berendsen, H. J. *J. Comput. Phys.* **1997**, *23*, 327.
26. Essman, V.; Perera, L.; Berkowitz, M. L.; Darden, T.; Lee, H.; Pedersen, L. G. *J. Chem. Phys.* **1995**, *103*, 8577.
27. Pastor, I. W. R.; Brooks, B. R.; Szabo, A. *J. Mol. Phys.* **1998**, *65*, 1409.
28. Humphrey, W.; Dalke, A.; Schulten, K. *J. Mol. Graphics* **1996**, *14*, 33.
29. Kollman, P. A.; Massova, I.; Reyes, C.; Kuhn, B.; Huo, S.; Lee, M.; Lee, T.; Duan, Y.; Wang, W.; Donini, O.; Cieplak, P.; Srinivasan, J.; Case, D. A.; Cheatham, T. E. *Acc. Chem. Res.* **2000**, *33*, 889.
30. Sitkoff, D.; Sharp, K. A.; Honig, B. *J. Phys. Chem.* **1994**, *98*, 1978.
31. Rocchia, W.; Alexov, E.; Honig, B. *J. Phys. Chem. B* **2001**, *105*, 6507.